Patient-Specific FE Analyses of Metatarsal Bones with Inhomogeneous Isotropic Material Properties

Nir Trabelsi[1a], Charles Milgrom[b], Zohar Yosibash[a]

[a]*Department of Mechanical Engineering, Ben-Gurion University of the Negev, Beer-Sheva, 84105, Israel*
[b]*Dept. of Orthopaedics, Hadassah Univ. Hospital, Jerusalem, Israel*

Abstract

The mechanical response of human metatarsal bones is of importance in both research and clinical practice, especially when associated with the correction of Hallux Valgus. Verified and validated patient-specific finite-element analysis (FEA) based on CT scans developed for human femurs are extended here to the first and second metatarsal bones.

Two fresh-frozen metatarsal #1 and five metatarsal #2 bones from three donors are loaded in-vitro at three different angles. Holes typical to Hallux Valgus correction are then drilled in the bones, which are then reloaded until fracture. In parallel, high-order FE models of the bones are created from CT-scans that mimic the experimental setting. We validate the FE results by comparison to experimental observations.

Excellent agreement is obtained with $R^2 = 0.99$ and slope of the regression line close to 1. We also compared the FE predicted fracture load and location for the second metatarsal bones with these measured in the experiment, demonstrating a good correspondence with approximately 10% difference. An accurate geometry and the assignment of inhomogeneous material properties are mandatory for the accurate predictions.

[1]Corresponding author. Present address: Department of Mechanical Engineering, Shamoon College of Engineering, Beer-Sheva, 84100, Israel. nirtr@sce.ac.il, Tel: +972-8-6475609.

After the FE predictions are validated, they are used to investigate the effect of drilled hole position, dimension and the insertion of a metallic device on the mechanical response so to optimize the outcome of the Hallux Valgus correction.

This study further substantiates the potential use of FEA in clinical practice.

Keywords: Metatarsal, Finite element analysis, p-FEM, Computed tomography (CT), Bone biomechanics.

1. Introduction

In non-trivial clinical cases, fracture risk assessment and pre-operative planning, patient-specific finite-element (FE) models are advocated [26]. A systematic process for reliable FE models of the human femur based on quantitative computed tomography (QCT) in a short timescale was presented in [28, 24, 25]. Our aim here is to extend the applicability of these FE methods to the the first and second metatarsal bones, and thereafter use the FE models to investigate the state of strains and risk of fracture due to holes drilled in MT bones for the correction of Hallux Valgus[2].

The metatarsal (denoted by MT) bones are a group of five bones in the foot located between the tarsal bones of the hind- and mid-foot and the phalanges of the toes. The first MT bone is of important biomechanical function within the foot, being a major weight-bearing structure. The second metatarsal is the longest and least robust metatarsal [19]. Most stress

[2]Enlargement of bone around the joint at the head of the big toe which in turn increases the angle between the first and second metatarsal bones.

fractures in the forefoot occur in the second MT [20]. Fracture of these bones also occurs following suture button fixation device used in the correction of Hallux Valgus [15]. Usually a polyethylene type suture and button construct are placed across the first and second MT bone's drilled holes. The optimal drill location, shape and size are of major interest to clinicians, and it is our aim to use FE methods to assist the surgeons in the decision of these parameters.

To the best of our knowledge the biomechanical response of MT bones have been scarcely investigated, and mostly based on either in-vitro or in-vivo experiments. In-vivo studies in [21, 4, 11] recorded the force acting during walking under the first and second MT heads. In [18] *in-vivo* axial strains were measured at the mid diaphysis of the second MT bone. Peak axial compression strains were larger than 2500 μstrain during treadmill walking and jogging and larger than 3000 μstrain in compression and tension during one and two-leg vertical jumps and broad jumping. This data is important to realize the magnitude of strains in normal activities in-vivo. In [7] fifteen cadaver feet were used for strain measurements on the second and fifth MT bones under different loading conditions. The peak vertical ground-reaction forces were 110% of body weight ($735 \pm 155N$). When the feet were loaded under normal walking conditions, the mean peak strain in the dorsal aspect of the second MT (-1897 μstrain) was more than twice that in the medial aspect of the fifth metatarsal.

Three osteotomies for Hallux Valgus correction were experimentally investigated in-vitro in [8] to determine the best one. Fifteen fresh-frozen cadaveric first MT bones were loaded in cantilever position (with an angle of

15^o to the ground surface) denoted as "physiological configuration". According to [8] this configuration is the most frequently used testing configuration, simulating the effect of the ground reaction force while standing. It was concluded that the chevron and the reversed-L osteotomies had a generally comparable mechanical response, with minimum alterations from that of the intact bone. An in-vitro study [19] demonstrated that bone density and not geometry is the major factor for the failure load of the second metatarsal bone.

Investigating MT bone's mechanical response by experiments involves various difficulties and limitations such as accurate loading conditions representation and a fair comparison between different metatarsal or different implant devices. To overcome these limitations, computational approaches, such as the FE method, are increasingly being applied. Any FE model aimed at clinical applications, requires a well verified and validated (V&V) protocol, i.e. that the FE results are free of numerical errors and furthermore match closely the experimental observations. V&V FE models allow a detailed and standardized sensitivity analysis of design parameters to guide strategies for the prescription of therapeutic footwear. In these FEMs one can isolate the parameters of interest, which is not always possible during experimentations.

Verified FE models validated by in-vitro experiments for the second MT bones are proposed herein. These FE models can quantify the deformation, stress, and strain distributions everywhere along the bones, and the influence of holes drilled and inserted implants can be easily investigated. In addition, the actual physiological loading situations are more difficult to mimic by in-vitro experiments than by a FE analysis. The scant number of available

FE studies on the MT bones are mostly unrealistic due to the assumptions that bone is homogeneous with a constant Young's modulus ranging between 7.3 − 17.0 GPa and Poisson ratio of 0.3 − 0.4 (see e.g. [5, 6, 17, 9, 10]). Furthermore, no studies are known that validate FE models of MT bones by experimental observations.

We extend the high-order patient-specific FE methods for femurs [28, 24, 25] to the first and second MT bones. Patient-specific FE models of the MT bones constructed from QCT scans with inhomogeneous isotropic material properties were loaded in a cantilever position at different angles. In parallel, experiments on the MT bones were performed (intact and after hole is drilled) and results were compared to the FE analyses. Once these FEMs were validated these were utilized to investigate the influence of location and position of the drilled hole on the mechanical response, and to determine the ability of the FEMs to predict the risk of fracture.

2. Material and methods

Three fresh-frozen isolated MT bones from two different Caucasian donors were used in our study; one first MT and two second MT bones as detailed in Table 1. The two second metatarsal bones were selected so they are as different in their material properties as possible (one which seems from the CT to be much denser than the other) and from an elderly and mid-age donors. The bones were determined to be free of skeletal diseases by inspecting the general medical history of the donor, and by inspecting X-ray scans to ensure that no bony lesions are present. Each metatarsal was defrosted, cleaned from soft tissue, QCT-scanned and thereafter exposed to in-vitro experiments during which loads and strains were measured. In the following, the experimental procedure is detailed and the methods for creating a high order FE model with inhomogeneous isotropic material properties are summarized.

Table 1: Summary on the MT bones in our study and donors details (* same donor).

Donor label	Side [Number]	Age (years)	Gender	Load limit in experiments [N]	Cause of death
$MT2Don39LT^*$	Left[2]	56	Male	100	Hepatic and renal failure
$MT2Don74LT$	Left[2]	75	Male	50	Dementia
$MT1Don39LT^*$	Left[1]	56	Male	200	Hepatic and renal failure

2.1. In-vitro biomechanical experiments

Several experiments were conducted on the two fresh-frozen human cadaver second MT bones and one experiment on the first MT bone to assess the mechanical response. The proximal portion of each metatarsal was cemented in a custom-designed jig (allowing clamping of the bone at different discrete inclination angles). Each sample was positioned with the dorsal side facing down to simulate bone state during standing. Thereafter QCT scans were performed using a Phillips Brilliance 16 CT (Eindhoven, Netherlands) with the following parameters: 120 kVp, 250 mAs, 1.25mm slice thickness, axial scan without overlap, and pixel size of 0.32mm.

Between six and eight uniaxial strain-gauges (SGs: Vishay C2A-06-125LW-350) were bonded to the surface of each MT at four anatomic locations: dorsal, plantar, medial, and lateral, see Figure 1.

The MT bones were loaded at 0^o, 15^o and 35^o tilt between the clamping jig to the ground surface to simulate three different phases of a gait cycle. Load

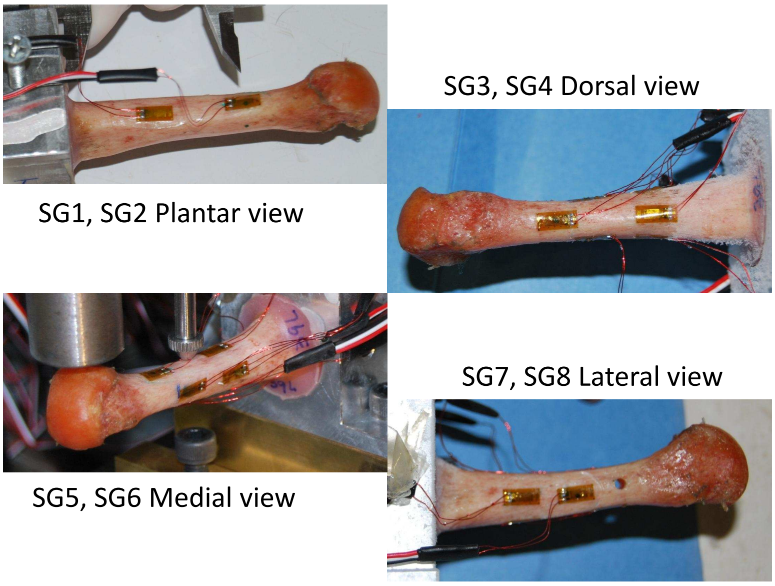

Figure 1: Strain-gauge (SG) locations.

was applied on the MT bone's head to mimic vertical ground-reaction forces (plantar to dorsal direction), see Figure 2(Right). At each inclination angle three or four consecutive monotonically loading-unloading patterns at a slow $(1/12, mm/sec)$ and a high $(2\,mm/sec)$ displacement rate were performed. Thereafter a hole of $\varnothing 2.5\,mm$ was drilled in the MT bones at a distal location about $40\,mm$ from the fixed surface - see Figure 2 (Left), and the tests were repeated.

Experiments started after the QCT scans (same day). Load was applied by a Zwick 1445 machine. During loading, strains and head displacements (measured by two linear displacements sensors) were collected at 100 Hz using a Vishey 7000 micro-measurements system. The maximum load was limited (see Table 1) to avoid bone fracture. The strains after 10s holding

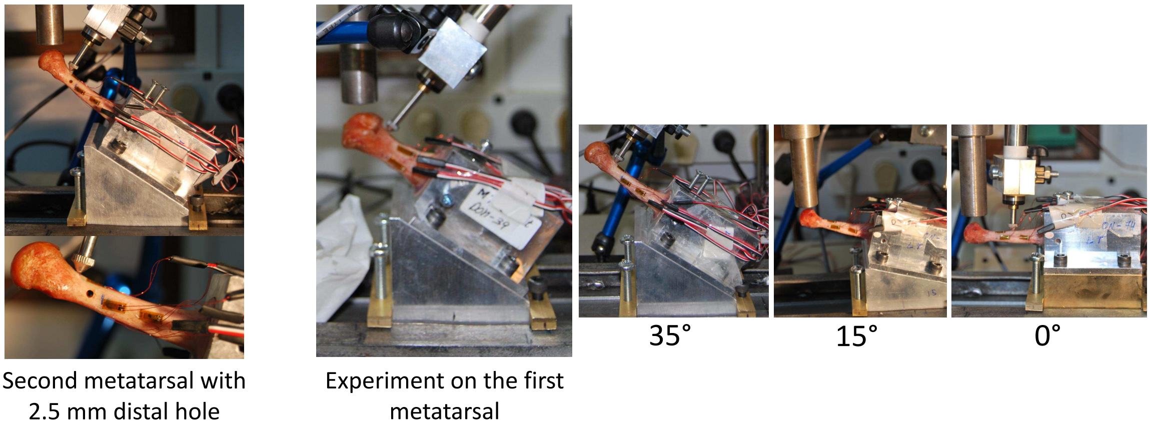

Figure 2: (Right) Experimental setup at 0^o, 15^o and 35^o tilt between the clamping jig to the horizontal surface-first and second MT bones. (Left) Experiment on the second MT with a hole drilled distally.

time at each test cycle were used to calculate a mean value of the test cycles per load step. These mean values were used for the comparison with FEA.

Following these experiments (intact and drilled MT bones), the second MT bones were loaded to fracture at a 15^o tilt configuration and at a constant displacement rate of $1/2\,mm/sec$. The main objective was to determine if the $2.5\,mm$ hole in the second MT bone affects the fracture location. Furthermore, the load at failure and location of failure on the surface were recorded.

2.2. Subject-specific high-order finite element models

The automatic 3-D reconstruction of the metatarsal geometry from QCT scans and generation of the p-version FE-meshes were based on an in-house program developed for femurs detailed in [28, 24] and briefly summarized herein. In the p-version of the FE method convergence is realized by keeping a fixed mesh and increasing the polynomial degree of the approximated solution. Therefore, the accurate geometrical description of the domain must be realized which is being accomplished by the use of blending-function mapping [22]. The geometry of the metatarsal was extracted from a QCT scan. Bone periosteal surface boundaries were traced at each slice and a points-cloud describing the surface was generated. A solid body was created based on the points-cloud. The metatarsal measured dimensions (section diameter and length) were compared to the geometric model used in the FE model resulting in a maximum difference of 0.4 mm (which is within the range of the CT resolution). The solid model was meshed by tetrahedral p-FEs using an auto-mesher. Typically a mesh of about 5000 tetrahedral elements was obtained having about 320,000 degrees of freedom at $p = 5$. The surfaces of the MT were accurately represented in the FE model by the blending mapping method [22]. The entire schematic algorithm for generating the metatarsal FE model is illustrated in Figure 3.

2.2.1. Boundary conditions applied on the FE model

The boundary conditions reflect the experimental set-up; A 100N force was applied on the metatarsal head according to the experiments: at 0°, 15°, 35° with respect to the horizontal plane. The distal face was fully constrained as presented in Figure 4.

2.2.2. Material properties assignment to the FE model

Material properties were demonstrated to have a major impact on the FE results of bones [28]. Empirical relations are available that estimate Young's modulus based on bone density, assuming a constant Poisson ratio. Many

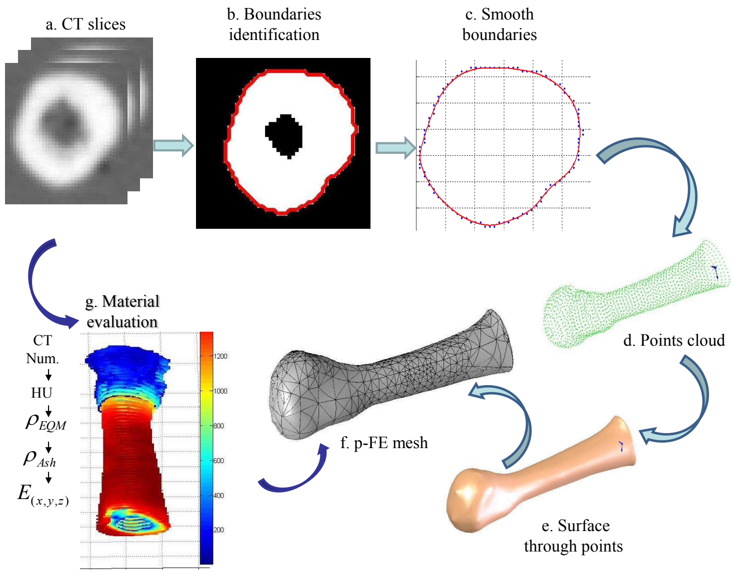

Figure 3: Schematic flowchart describing the generation of the p-FE model from QCT scans. a - Typical CT-slice, b. - Contour identification, c. - Smoothing boundary points, d. - Points cloud representing the bone surface. e. - Bone surface, f. - p-FE mesh and g. - Material evaluation from CT data.

of these relations exist - for example, a total of 18 studies and 22 elasticity-density relations are summarized in a recent literature review [12]. Despite the vast amount of studies, none is specific to the metatarsal's material properties. Here we adopted the material evaluation procedure developed for the femur [28, 24, 25]. The material mapping strategy from the QCT data to the FE model first employs a noise reduction algorithm by boundary correction and moving average (accounting for the partial volume effect and smooth the material data) and evaluates Young's modulus directly from the QCT slices at each required integration point (see illustrations in Figure 3-g and section

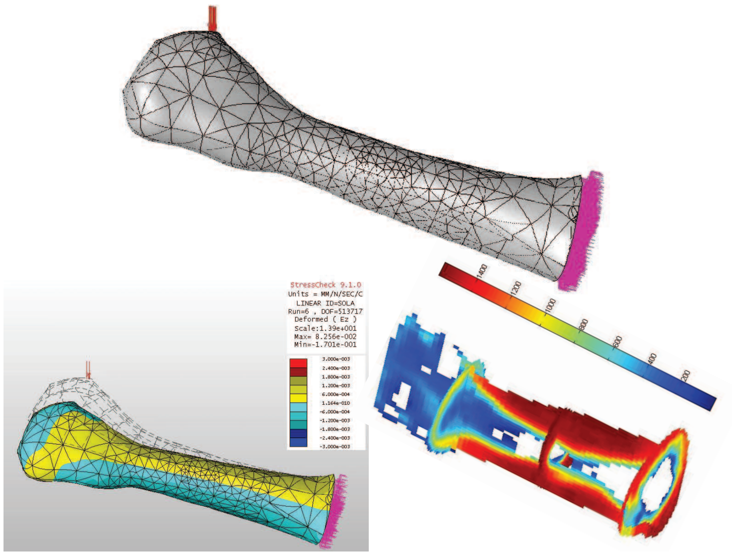

Figure 4: Boundary conditions applied to the FE model and section view to observe the density distribution in the second MT bone.

view of the density distribution in Figure 4). A linear elastic isotropic heterogeneous Young's modulus was determined based on the QCT data (Poisson ratio is kept constant at $\nu = 0.3$).

The pointwise Young's modulus was determined as follows: Five calibration phantoms (with different concentration of K_2HPO_4 ranging from 0 to 300 mg/cm^3) were placed around the metatarsal bones during the CT scan. The CT numbers of these phantoms (Hounsfield Units- HUs) were correlated to the mineral density ρ_{EQM} according to the linear relation (1) (see for details [3]). The mineral density ρ_{EQM} is associated with bone's ash density ρ_{Ash} according to (2), see [16], and the later determines the Young's modulus E_{Cort}, E_{Trab} (cortical and trabecular) according to (3)-(4) (see also [14]). These relationships were found to provide an excellent match between the p-FE analyses and experiments for the proximal femur, see [28, 24].

$$\rho_{EQM} = 10^{-3}\,(a \times HU + b) \quad [g/cm^3] \tag{1}$$

$$\rho_{Ash} = (1.22 \times \rho_{EQM} + 0.0523) \qquad [g/cm^3] \tag{2}$$

$$E_{Cort} = 10200 \times \rho_{Ash}^{2.01} \qquad [MPa] \tag{3}$$

$$E_{Trab} = 5307 \times \rho_{Ash} + 469 \qquad [MPa] \tag{4}$$

No exact HU exists that distinguishes between the cortical and trabecular regions. The differentiation between cortical and trabecular bone was determined following [1, 2] and the experience gained in our previous works. We associated voxel values of $HU > 600$ (ash $density > 0.6g/cm^3$) with the cortical bone and values of $HU \leq 600$ to the trabecular bone. The bone marrow in the cavity had constant material properties with $E = 0.5\,GPa$ and $\nu = 0.49$ (almost incompressible). A change in E in the range of 0 to a 0.5GPa for the bone marrow cavity had a negligible effect on the strains. The assignment of $E(x, y, z)$ at each integration point (512 Gauss points for a tetrahedral element) was determined according to the density recorded by the CT scan.

To quantify the influence of an inhomogeneous Young modulus versus a constant value on the results, and to justify the necessity of an inhomogeneous E, a comparison between several FE models was conducted: in addition to the inhomogeneous E, we assigned to the same FE models three distinct constant values of 7.3, 12 and 17 GPa, with a Poisson ratio 0.3 covering the range used in other studies.

2.2.3. Verification and validation of the FE model

All FE results (the global error in energy norm and strain values at the points of interest (POI)) were verified, i.e., the polynomial degree p over the FEs was increased until convergence.

After verification, the FE principal strains were computed for each SG-location by averaging the value on elements' surface, and the principal directions were verified to align along the SG-directions in the experiments. The averaged strain accounts for the SG gauge length (the SG measures an average value over the gauge length). The agreement between FE result and experimental observation was determined by a regression analysis. The quality of the FE analyses was expressed by the coefficient of linear regression R^2, and by the slope and the intercept of the regression curve, following [23].

2.2.4. Failure prediction by the FE model

A linear response between strains and applied load was usually observed until fracture [13] on the global scale, therefore it is conceivable to use linear FE analyses to predict the load magnitude and failure location at fracture. Fracture was determined by the maximum principal strain criterion [2], i.e. where the average principal strain (averaged over a 2 mm length - as the gauge of a strain gauge) in tension on the cortical surface reaches 7300 ± 500 μstrain (see also [27]).

Due to clamping the distal face of the MT bones in the FE analysis, the strains at the intersection of the bone surface and clamped surface were singular, therefore we inspected elements away from the clamped-free surface interface. The failure location is the area at which the average maximum principal strains on bone's surface is highest, and the predicted failure load was computed by:

$$\frac{Max.\ avg.\ principal\ FE\ strain}{7300} \times\ Applied\ load\ in\ FEA. \qquad (5)$$

2.3. The influence of the location and diameter or the drilled hole on the mechanical response

The strains computed by the FE model of the MT bones with the drilled hole were compared to the ones measured in the in-vitro test for validation purposes. Following the validation step, the FE models were used to identify the strain intensification at the borders of the drilled holes.

After validation of the FE models, they were used to investigate the influence of the location and diameter of the drilled hole on the mechanical response. The conflicting demands to insert the hole in the most distal part on one hand, and the progressive softening of material properties towards the distal part on the other hand, require an optimized solution that is being determined by the FE model.

The FE models were also used to determine the influence of a surgeon error by drilling the hole in an offset from the targeting attempts (a 5 degrees offset from the horizontal plane). Finally, the influence of the metallic sleeve placed inside the hole on the strains in the second MT bone was examined. For these purposes we performed numerical investigation for each MT bone at six different configurations, see Figure 5. These included:

a) $\varnothing 2.5\,mm$ hole located $35\,mm$ distally to the fixed surface.

b) $\varnothing 2.5\,mm$ hole located $40\,mm$ distally to the fixed surface- Reference model.

c) $\varnothing 2.5\,mm$ hole located $45\,mm$ distally to the fixed surface.

d) $\varnothing 2.5\,mm$ hole drilled with a 5 degree horizonal shift at the starting drilled points (medial) to end point (lateral) and located 40mm distally to the fixed surface.

e) $\varnothing 1.5\,mm$ hole located $40\,mm$ distally to the fixed surface.

f) Model b) with a metallic sleeve placed inside the hole.

All models were placed at a 0^o tilt angle. The strains at SGs location and at the hole medial and lateral edges were compared to the reference model b).

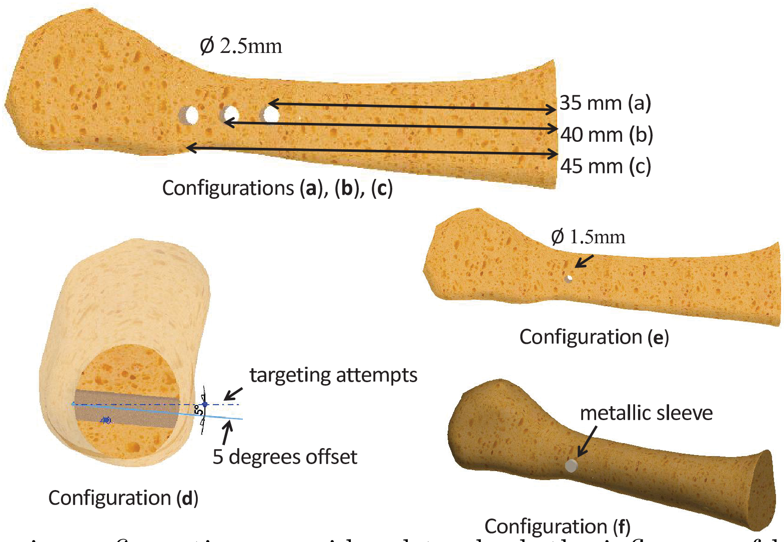

Figure 5: The six configurations considered to check the influence of hole's position.

3. Results

3.1. Experimental results

In most experiments a linear response ($R^2 > 0.98$) between force and strains was observed beyond a $5N$ pre-load. Some SGs bonded at the medial and lateral sides provided too small strains due to their location close to the neutral axis.

Measured strains demonstrated a high repeatability for the repeated loads with standard deviations of $0 - 5\%$. Any experimental observation having a nonlinear response, a standard deviation larger than 10% or strains below 100 μstarins was discarded from our investigation (all of these occurred at the medial and lateral side and close to the neutral axis). The applied load rate had almost no influence on the strain measurements. For the $0°$ load, the peak strains at $100\,N$ load in the dorsal and plantar sides of the intact second metatarsal were obtained for MT Don74LT: -2707 and 2995 μstrain respectively, at the proximal part (SG1, SG3).

Comparing the mechanical response of the intact MT bones and the MT bones with holes, the global response was not significantly influenced by the $\varnothing$2.5 mm distal hole (with mean absolute error of 6.5%). The SGs in the vicinity of the hole (SG2 and SG4) showed a more pronounced influence between the intact MT and the one with the hole with mean absolute error of 13%. The maximum difference in strain measurements was observed for SG2 and reached up to 26% for MT bone Don74LT and 10% for MT bone Don39LT.

A significant difference in the strains was found between the second MT bones Don39LT and Don74LT with an average factor of almost two. Also as expected, the strains observed for the second MT bones were considerably higher than these in the first MT bone.

The head displacement was also measured to assure that the small displacement assumption inherent in the linear elastic FE analysis is justified. The mean head displacement value for the second MT bone was $0.5\,mm$ (less than 1% compare to the metatarsal length). Moreover, most of the displacement was caused by compression of the cartilage.

To investigate if the considerable difference in the mechanical response between the two second MT bones may be explained by geometrical measures, we summarize in Table 2: (a) MT bone length from the clamped proximal end, (b) locations of minimum cross-section (approximate location of SG2, SG4), (c) lateral-medial minimum cross-section diameter (d) dorsal-plantar minimum cross-section diameter. Since the influence of the geomet-

Table 2: Geometric parameters of the tested metatarsals.

	MT2Don39LT	MT2Don74LT	MT1Don39LT
Length- clamped to end [mm]	68	64	52
Locations of minimum cross-section [mm]	41	42	26
Minimum diameter lateral-medial [mm]	8.6	8.1	16.6
Minimum diameter dorsal-plantar [mm]	9.5	7.9	14.5

rical parameters can only partially explain the strain differences obtained for Don39LT and Don74LT, we postulate that the substantial different material properties distribution in the two MT bones affected strongly the mechanical response.

3.1.1. Fracture experiments

Load until fracture was applied to the two second MT bones with holes. The SGs were monitored to assure that at $100N$ load same strains as in the static experiments are obtained (difference of less than 5% observed). Fracture in both bones occurred close to the PMMA as shown in Figure 6 with no visual evidence of fracture or damage near the holes. A linear response

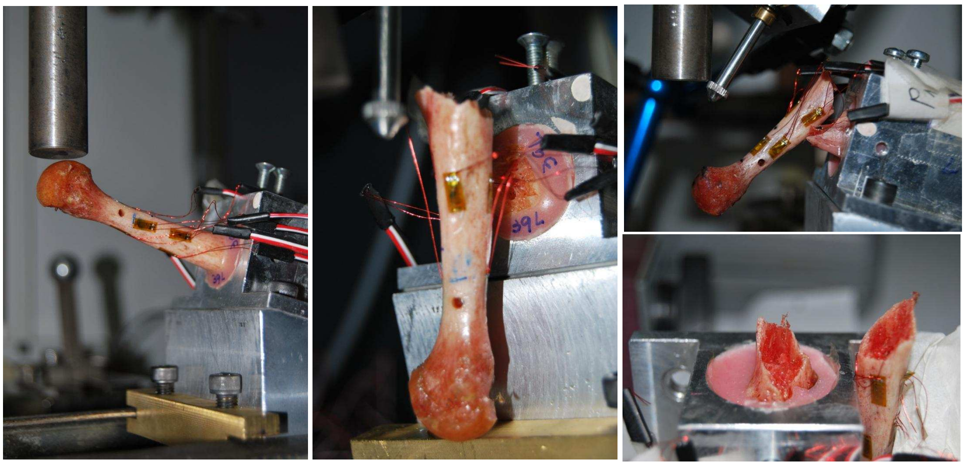

Figure 6: Fractures in second metatarsal bones.

between strains and load was observed for the SGs close to the fracture location almost until fracture as seen in Figure 7. Close to the fracture one may notice also a "jump" in the load, attributed to a slip of between the bone and machine punch (strain is not changed but load decreases due to the displacement controlled experiment). The fracture load as well as maximum strains at fracture are summarized in Table 3. The maximum tensile strain ratio at failure between MT2Don39LT and MT2Don74LT is 1.23 whereas the

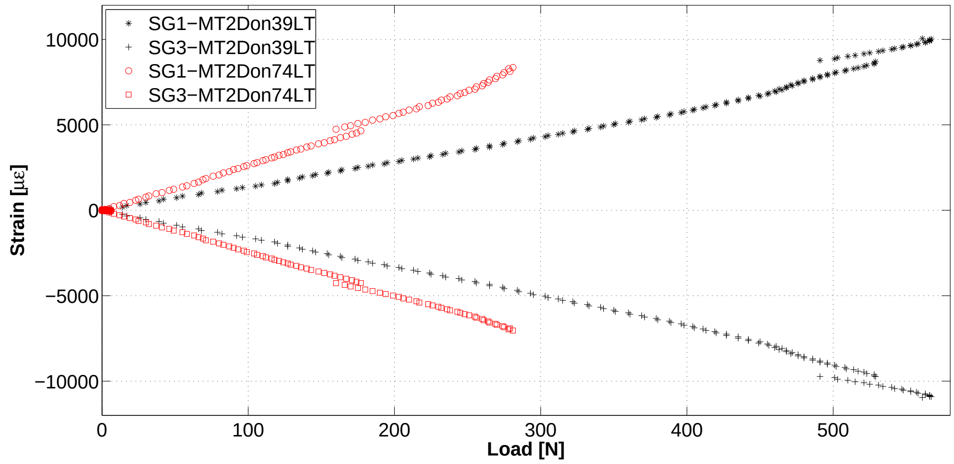

Figure 7: Strains vs. load at plantar and dorsal sides close to proximal clamping in second MT bones until fracture.

Table 3: Maximum strains and load at fracture.

	MT2Don39LT	MT2Don74LT
SG1 $[\mu\varepsilon]$	9619	7819
SG2 $[\mu\varepsilon]$	7133	6784
SG3 $[\mu\varepsilon]$	-10660	-6716
SG4 $[\mu\varepsilon]$	-9707	-5835
Load at fracture $[N]$	560	270

fracture load ratio is 2.07.

3.2. FE results

A typical example of the convergence patterns is shown in Figure 8.

Following the verification process the FE strain results were validated by

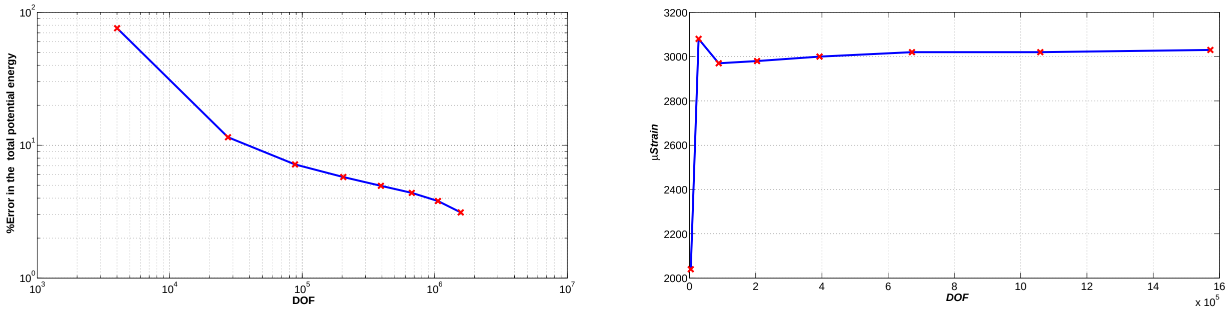

Figure 8: Convergence of the relative error in energy norm (left) and strain at a representative POI (right) in MT2.

comparison to the experimental observations.

Head displacements were also compared to the FE results. However, since the cartilage in the MT bone's head was not modeled, the local displacements which are mainly affected by the compression of the cartilage, yielded always a smaller value of about 70% compared to the experimental observations. This information is reported herein for the sake of completeness.

Figure 9 shows the agreement between p-FE analysis result and in-vitro experiments for the intact MT bones (right) and for second MT bones with the 2.5 mm distal hole (left). Each point on the plot represents the strain values extracted from the FE models (Y-axis) and the one observed in the experiment (X-axis) on specific location and tilt angle. All FE strains were check for convergence with maximum relative error of 0.5% used as a criteria for the FE simulations. A detailed comparison between the largest absolute strains at the relevant points of interest (POIs) and experimental observations at the three angles is presented in Figure 10. One may also observe the effect of the hole in the second metatarsal by comparing the values extracted

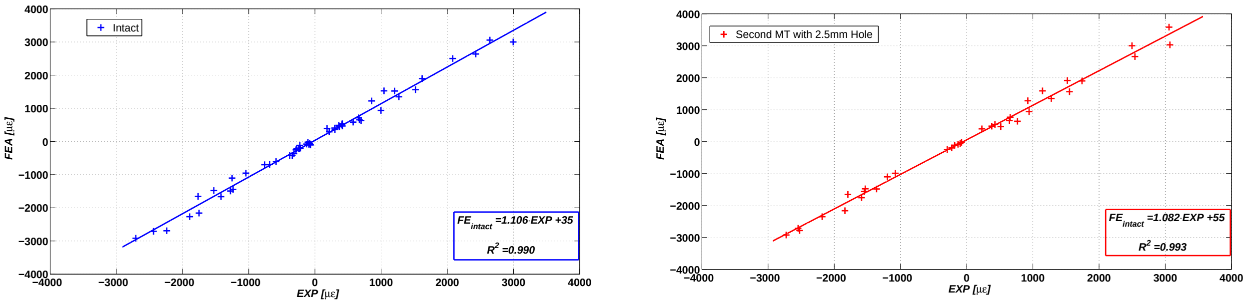

Figure 9: Regression lines between p-FE results and in-vitro experiments, for the intact first and second metatarsals (left) and for second metatarsals with the ∅2.5 mm distal hole (right).

from both experiments and FE analyses. The errors between the FE strains and the measured ones have a mean absolute value of 13% with a slope of the regression curve of 0.99. The poorer agreement between the FEA and experiment was observed in location SG2 (in particular for donor 39), but the difference between intact and the bone with a hole is the same in both FEA and experiments. A significant difference in the stiffness between the bones Don39LT and Don74LT was observed in experiments as well as in the FEA.

The distal hole located close to the neutral axis had a very local influence on the mechanical response which seems to have no influence on the risk of fracture. Since we could not measure the strains at the hole location, the local influence can only be investigated by the FE results.

We found that the strain around the hole is at the same order or magnitude compared to the strains at the MT surface or at the proximal part (around 1600 μstrain for MT2Don39LT and 3000 μstrain for MT2Don74LT).

However, the bone density (and thus the ultimate strain) are smaller in the vicinity of the hole (Figure 4 right) and one must take both parameters into consideration; maximum strain and bone density.

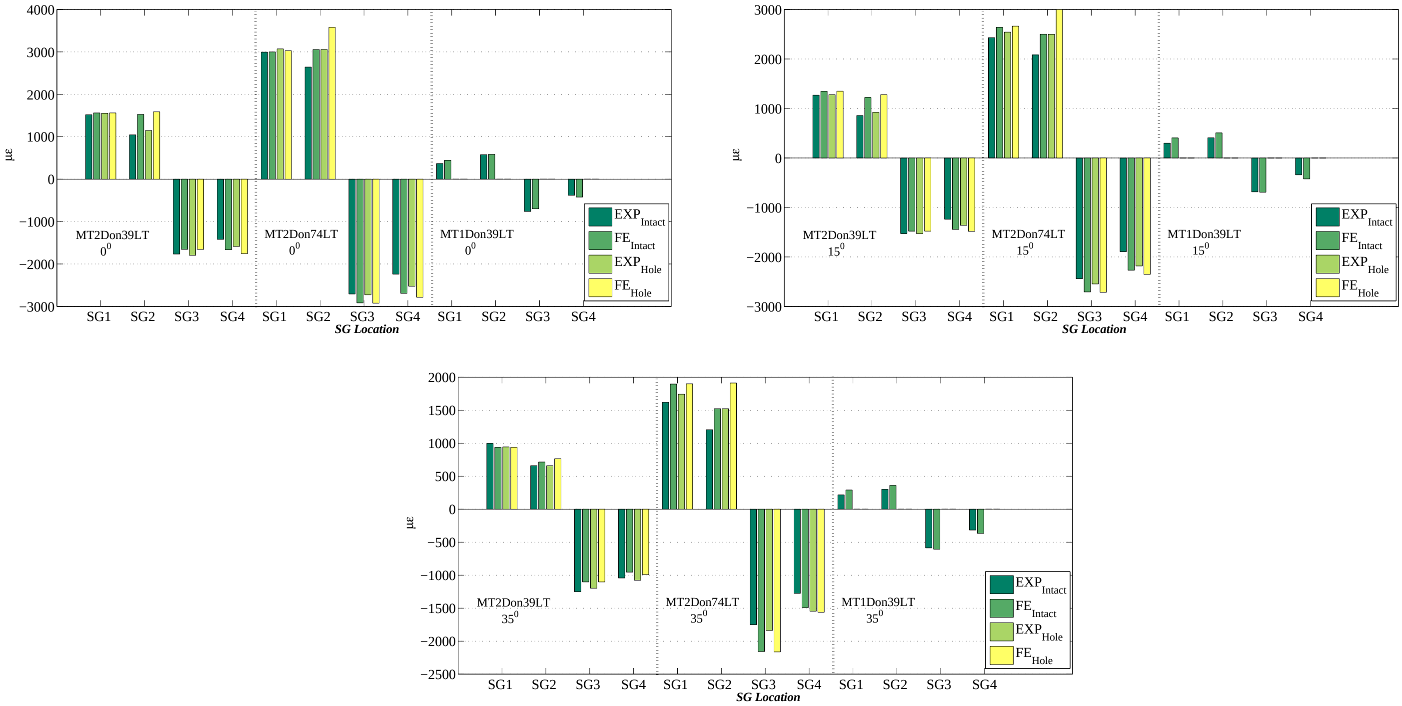

Figure 10: Comparison of strains computed by the FEA and these measured experimentally (SG1-4) for the three MT bones.

Remark 1. *Applying a constant Young modulus throughout the entire metatarsal bone in the FE analysis (as performed in several past studies for simplification) results in large deviations in the predicted strains compared to experimental observations (see Appendix [**?**]).*

Influence of the hole location: After verification and validation, FE models were created for each of the two second MT bones in the six configurations a)-f) in subsection 2.3 (shown in Figure 5). The maximum principal strains (tension and compression) at the lateral and medial hole edge were extracted and used for comparison purposes to the reference FE configuration b) ($\varnothing 2.5\,mm$ hole located $40\,mm$ distally to the fixed surface). The difference in percentage with respect to configuration b) is presented in Figure 11(top) for MT2Don39LT and 11(bottom) for MT2Don74LT. One may observe that the more distally the hole is placed the higher the strains although the decrease in the moment. Considerable effect is due to "surgeon's error" in which the hole lateral edge is at an offset of 5^o from the horizontal plane.

Inspecting the strains at SGs location for the six cases show no significant difference, with a maximum difference of at most 10% at SG2 and SG4 (the vicinity of the hole) .

FE prediction of the fracture load:

The maximum average principal strain in FE model at 15^0 was obtained close to the clamped surface: 1470 μstrain for MT2Don39LT and 2933 μstrain for MT2Don74LT for a 100 N load. Using (5) the estimated load at fracture is 497 ± 34 N for MT2Don39LT (compared to 560 N in the experiment, a 11% difference) and 249 ± 17 N for T2Don74LT (compared to 270 N in the experiment, a 8% difference). The estimated location of fracture is in the plantar region (as in the experiment) about 7 mm from the clamped surface for MT2Don39LT and about 4 mm for MT2Don74LT (very close to the fracture in the experiment).

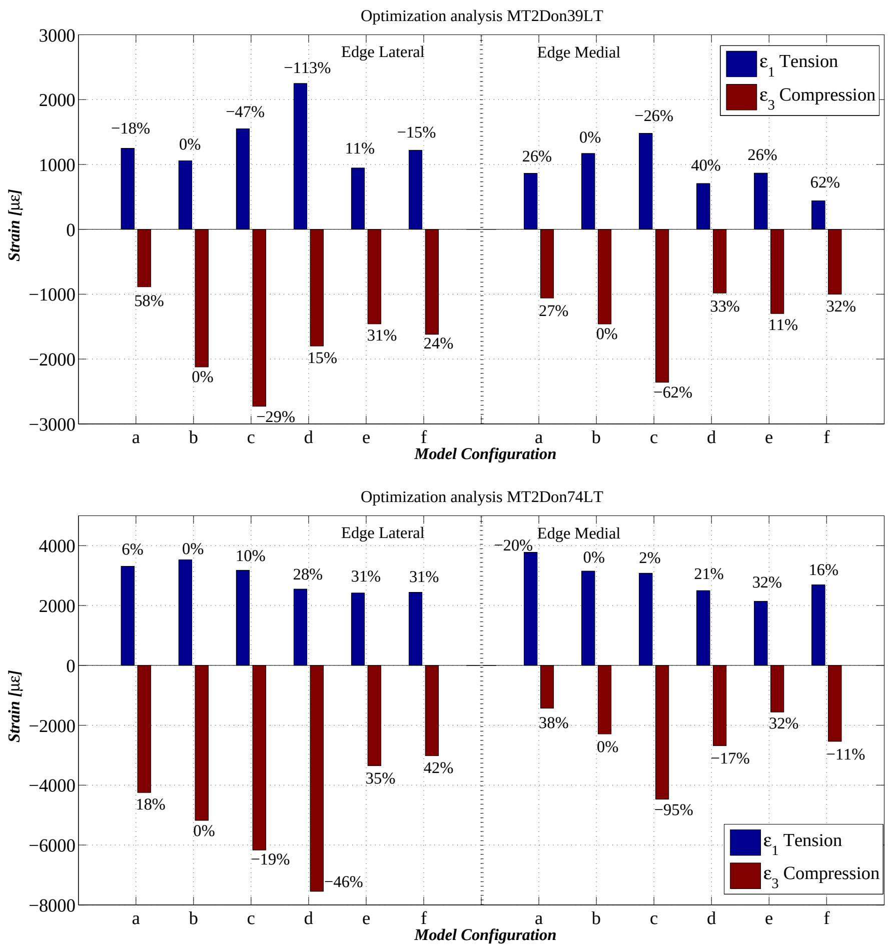

Figure 11: Difference in min/max principal strain at the hole circumference compared to configuration b) at 0^o to check the influence of hole's position. Top, MT2Don39LT. Bottom, MT2Don74LT.

4. Discussion

Patient-specific FE models of long bones as the femur and tibia, generated from QCT data, have become of interest because of their high potential in clinic practice usage. Here, the “reliability” of such patient-specific p-FE models for the metatarsal bones was investigated. The terminology ”reliable FE models” is used when the FE results satisfy three conditions: (a) They were verified, i.e. the numerical errors are under control. This means that the relative error in energy norm of the overall model is guaranteed to be small and the data of interest has shown to converge. (b) The FE models have been validated, i.e. the computed values at several locations have been compared to experimental observations and show good correlation. (c) Different FE models constructed according to the same algorithm were verified and validated on a large number of experiments performed on bones harvested from different donors. In this study a small cohort of MT bones was tested, and this condition is not fulfilled in full.

MT fracture is one of the most common foot injuries and an improved understanding of the MT bones mechanical response under different loads by FE models may provide an important tool for the diagnosis and prevention of such injuries. These FE capabilities also assist orthopedic surgeons in cases of correction of Hallux Valgus or to predict fractures that may result following the insertion of metal implants.

The p-FE simulated mechanical response of the first and second MT bones was first verified and thereafter compared to experimental observations perform on three fresh frozen MT bones. A very good agreement was obtained between the FE strains and the experimental observations for all inclination angles with $R^2 = 0.99$ and slope of the regression line close to 1. We found that both inhomogeneous material properties and geometry significantly affects the strains (and as a result the stresses) along the MT bones. This study demonstrates that inhomogeneous material properties are necessary (unlike the constant ones used in past studies performed on the MT bones) for a reliable FE model. The maximum Young's modulus may have values up to 20GPa with an average value of about 7GPa. The results of this study show that the second metatarsal experience significantly higher strains than the first MT bone under the same load due to the longer moment arm, increasing the bending stresses and the smaller cross-section and density distribution along the metatarsal. In addition two different second MT bones show significant difference in the strain to load relationship due to differences in the density spatial distribution. Although the number of specimens in this study is small it can demonstrates the wide distribution of bones mechanical response within the human bodies.

We also investigated the influence of a distally located hole of ∅2.5 mm in the second MT bones. It was concluded that the global response is not significantly influenced by a ∅2.5 mm hole but from the clinical view-point the exact location of the hole has to take into consideration the local material properties distribution and cross-section diameter. The presence of the distal hole of a diameter of ∅2.5 mm was shown in the in-vitro experiment not to influence the location of the fracture and the p-FE analysis demonstrated that the local strains at fracture around the hole are considerably lower than at the proximal part where the fracture occur. It was demonstrated by the FE analysis the effect of "surgeon's error" (hole's lateral edge is at an offset of 5^o from the horizontal plane). In this case the strains along the hole's surface may increase considerably compared to the proper horizontal plane, that in turn may lead to fracture.

Finally, the prediction of the fracture load and location by a linear FEA using the maximum average principal strains is in a very good agreement with the experimental observation. Quantitatively, this agreement is within 10%, although a slight nonlinear response is evident in the experiment at loads close to the fracture load.

Our conclusions suggest that surgery procedures on MT bones may easily be optimized by performing a local QCT scan of patient's foot followed by a fast p-FE analysis.

Limitations of the present work are: (a) The FE models have been validated on a small cohort of three normal metatarsal bones in-vitro. (b) The FE model did not take into account the known anisotropic relationship of the bone tissue. (c) Young's modulus to density relation used in this study is based on experiments which were not preformed on the MT bone. (d) The boundary conditions do not accurately reflect the physiological loading.

To conclude, this study demonstrates the ability to apply p-FE methods to analyze patient-specific metatarsal bones with inhomogeneous isotropic material properties. The methods were numerically verified and validated by experimental observations. The entire simulation (CT to FE model) lasts less than an hour, demonstrating the high level of automation. The p-FE models may be used to provide a more depth insight into the mechanical response of metatarsal bones. The ability to perform a valid numerical comparison can be utilized to investigate the influence of fixation devices and to optimize theirs shape and location for specific patients.

Conflict of interest

NT, CM and ZY have no conflict of interest to declare that could bias the presented work. RH was the CEO of BoneFix (BoneFix funded a small part of the study) at the time when the experiments were performed. For more than a year he is no longer associated with BoneFix.

Acknowledgements

NR and ZY gratefully acknowledge the generous support of the Technical University of Munich - Institute for Advanced Study, funded by the German Excellence Initiative.

CM and ZY gratefully acknowledge the partial support of this work by the Chief Scientist Office of the Ministry of Health, Israel under grant no. 293 3-00000-7375.

Competing interests: None declared

Funding: Partial support was provided by: IAS-TUM, Germany, Chief Scientist Office of the Ministry of Health, Israel, Bonfix LTD, Israel.

Ethical approval: Not required

Appendix A. Influence of inhomogeneous Young's modulus on FE results

Different Young's moduli influence significantly FEA results and the stiffness of the bone. Higher Young's moduli decreases the strains and displacements in the bone. We illustrate here on the basis of randomly selected three metatarsal bones the necessity of an inhomogeneous (density dependent) Young's modulus in the FE simulations. The mean absolute value of the difference between the FE strains compared to the experiment for each bone (in percentage) is summarized in Table A.4: Whereas a specific con-

Table A.4: Mean difference in strains between FE models and experiments at 15^o - Inhomogeneous versus homogeneous constant E.

Bone	Inhomogeneous E	$E = 7.3$ GPa	$E = 12$ GPa	$E = 17$ GPa
MT1Don39LT	18%	55%	27%	39%
MT2Don39LT	19%	117%	49%	27%
MT2Don74LT	14%	85%	20%	21%
Avg all MTs	17%	86%	32%	29%

stant Young's modulus may represent well one MT bone, the same constant Young's modulus results in a much poorer agreement for another MT bone.

[1] Alho, A., Husby, T., Hoiseth, A., 1988. Bone mineral content and mechanical strength. An ex-vivo study on human femora and autopsy. Clin. Orthop. 227, 292–297.

[2] Bayraktar, H., Morgan, E., Niebur, G., Morris, G., Wong, E., Keaveny, M., 2004. Comparison of the elastic and yield properties of human femoral trabecular and cortical bone tissue. J. Biomech. 37, 27–35.

[3] Cann, C., 1988. Quantitative CT for determination of bone mineral density: A review. Radiology 166, 509–522.

[4] Chen, W. M., Vee-Sin Lee, P., Park, S. B., Lee, S. J., Phyau Wui Shim, V., Lee, T., 2010. A novel gait platform to measure isolated plantar metatarsal forces during walking. J. Biomech. 43 (10), 2017–2021.

[5] Chen, W. P., Tang, F. T., Ju, C. W., 2001. Stress distribution of the foot during mid-stance to push-off in barefoot gait: a 3-d finite element analysis. Clinical Biomechanics 16 (7), 614–620.

[6] Cheung, J. T., Zhang, M., Leung, A. K., Fan, Y. B., 2005. Three-dimensional finite element analysis of the foot during standing–a material sensitivity study. J. Biomech. 38 (5), 1045–1054.

[7] Donahue, S. W., Sharkey, N. A., 1999. Strains in the metatarsals during the stance phase of gait: implications for stress fractures. J. Bone & Joint Surg Am. 81 (9), 1236–1244.

[8] Favre, P., Farine, M., Snedeker, J. G., Maquieira, G. J., Espinosa, N., 2010. Biomechanical consequences of first metatarsal osteotomy in treating hallux valgus. Clinical Biomechanics 25 (7), 721–727.

[9] Garcia-Aznar, J. M., Bayod, J., Rosas, A., Larrainzar, R., Garcia-Bogalo, R., Doblare, M., Llanos, L. F., 2009. Load transfer mechanism for different metatarsal geometries: a finite element study. J. Biomech. Engrg. 131 (2), 021011–1–021011–7.

[10] Gu, Y. D., Ren, X. J., Li, J. S., Lake, M. J., Zhang, Q. Y., Zeng, Y. J., 2010. Computer simulation of stress distribution in the metatarsals at different inversion landing angles using the finite element method. International Orthopaedics 34 (5), 669–676.

[11] Hayafune, N., Hayafune, Y., Jacob, H. A. C., 1999. Pressure and force distribution characteristics under the normal foot during the push-off phase in gait. The Foot 9 (2), 88–92.

[12] Helgason, B., Perilli, E., Schileo, E., Taddei, F., Brynjolfsson, S., Viceconti, M., 2008. Mathematical relationships between bone density and mechanical properties: A literature review. Clinical Biomechanics 23, 135 – 146.

[13] Juszczyk, M. M., Cristofolini, L., Viceconti, M., 2011. The human proximal femur behaves linearly elastic up to failure under physiological loading conditions. J. Biomech.In press, doi:10.1016/j.jbiomech.2011.05.038.

[14] Keller, T. S., 1994. Predicting the compressive mechanical behavior of bone. J. Biomech. 27, 1159–1168.

[15] Kemp, T. J., Hirose, C. B., Coughlin, M. J., 2010. Fracture of the second metatarsal following suture button fixation device in the correction of hallux valgus. Foot and Ankle International 31 (8), 712–716.

[16] Keyak, J., Falkinstein, Y., 2003. Comparison of in situ and in vitro CT scan-based finite element model predictions of proximal femoral fracture load. Med. Eng. Phys. 25, 781–787.

[17] Kristen, K. H., Berger, K., Berger, C., Kampla, W., Anzbock, W., Weitzel, S. H., 2005. The first metatarsal bone under loading conditions: a finite element analysis. Foot and Ankle Clinics of North America 10 (1), 1–14.

[18] Milgrom, C., Finestone, A., Sharkey, N., Hamel, A., Mandes, V., Burr, D., Arndt, A. Ekenman, I., 2002. Metatarsal strains are sufficient to cause fatigue fracture during cyclic overloading. Foot and Ankle International 23 (3), 230–235.

[19] Muehleman, C., Lidtke, R., Berzins, A., Becker, J. H., Shott, A., Sumner, D. R., 2000. Contributions of bone density and geometry to the strength of the human second metatarsal. Bone 27 (5), 709–714.

[20] Sharkey, N. A., Ferris, L., Smith, T. S., Matthews, D. K., 1995. Strain and loading of the second metatarsal during heel-lift. J. Bone & Joint Surg Am. 77, 1050–1057.

[21] Stokes, I. A., Hutton, W. C., Stott, J. R., 1979. Forces acting on the metatarsals during normal walking. J. Anatomy 129 (3), 579–590.

[22] Szabó, B. A., Babuška, I., 1991. Finite Element Analysis. John-Wiley, New York.

[23] Taddei, F., Cristofolini, L., Martelli, S., Gill, H., Viceconti, M., 2006. Subject-specific finite element models of long bones: An in vitro evaluation of the overall accuracy. J. Biomech. 39, 2457–2467.

[24] Trabelsi, N., Yosibash, Z., Milgrom, C., 2009. Validation of subject-specific automated p-FE analysis of the proximal femur. J. Biomech. 42 (3), 234–241.

[25] Trabelsi, N., Yosibash, Z., Wutteb, C., Augat, R., Eberle, S., 2011. Patient-specific finite element analysis of the human femur - a double-blinded biomechanical validation. J. Biomech. 44 (9), 1666–1672.

[26] Viceconti, M., Davinelli, M., Taddei, F., Cappello, A., 2004. Automatic generation of accurate subject-specific bone finite element models to be used in clinical studies. J. Biomech. 37, 1597–1605.

[27] Yosibash, Z., Tal, D., Trabelsi, N., 2010. Predicting the yield of the proximal femur using high order finite element analysis with inhomogeneous orthotropic material properties. Philosophycal Transaction of the Royal Society: A 368, 2707–2723.

[28] Yosibash, Z., Trabelsi, N., Milgrom, C., 2007. Reliable simulations of the human proximal femur by high-order finite element analysis validated by experimental observations. J. Biomech. 40 (16), 3688–3699.